Inverse Problems in Population Balances: Growth and Nucleation from Dynamic Data

Alan W. Mahoney
School of Chemical Engineering, Purdue University. West Lafayette, IN 47907

Francis J. Doyle, III
Dept. of Chemical Engineering, University of Delaware, Newark, DE 19716

Doraiswami Ramkrishna
School of Chemical Engineering, Purdue University. West Lafayette, IN 47907

Particulate process modeling is critical for system design and control used widely in the chemical industry. Previous methods have focused on the assumption of appropriate models that can capture system behavior. A new technique presented is based on viewing the population balance from an inverse problem perspective that allows to determine appropriate models directly from experimental data. Under suitable assumptions (deterministic growth rate, no aggregation), the population balance equation may be solved by the method of characteristics, which associates the number density for any size at any time with a single point from the initial or boundary condition. The key to using this is the recognition that these characteristics correspond to the size history of individual particles and can be associated with constant cumulative number densities (quantiles) of the population. These quantiles are easily identifiable from experimental data. The variation of size and number density along these characteristics provides decoupled equations used to determine the growth rate. Validity of the determined growth law is checked by the collapse of the experimental data onto initial and boundary conditions.

Introduction

The value of the products is affected by the particle-size distribution (PSD) in a number of ways. Properties that depend directly on the distribution can be of key importance in preventing segregation in consumer particle mixtures, producing coatings with desired mechanical (coverage/stickiness) and optical (gloss, brightness) properties, controlling the surface reaction or dissolution rate (total alkalinity of lubricant additives, dosage rate of pharmaceutical particles), and controlling the rheology of formulated products. The size distribution also affects the dynamics of other key variables in reactors, especially crystal purity and habit. Finally, the PSD affects cost of processing, affecting transfer speed, and especially filtration rates, a large component of powder processing.

Particulate systems involve individual particle phenomena such as aggregation, breakage, nucleation and growth, coupled through continuous phase reactions and transport. Understanding the inherent complexity in these systems is essential for the construction of appropriate models. Many approaches are often either oversimplified and unable to capture essential system dynamics, or complex beyond the availability of experimental data. The approach pursued here is a gray-box approach, recognizing the full population balance model structure, but treating individual particle processes as unknown functionalities to be determined through modeling.

Current modeling of particulate processes can be separated into classes: first principles, black-box, direct observation, parameter estimation, and inverse problem techniques. These have various strengths and weaknesses that will be investigated in turn. We will see that these methods do not provide for the elucidation of fundamental system behavior directly from experimental data.

The physics literature is especially rich in first principle models for growth, nucleation, and aggregation. Prevalent

Correspondence concerning this article should be addressed to D. Ramkrishna.

growth models include diffusion limited growth, spiral dislocation growth, and surface polynucleation (House, 1981; Nielsen, 1984; Taiet et al., 1992). Nucleation models include primary nucleation as the formation of 1-mers, 2-mers under dynamic equilibrium conditions (Gómez-Morales et al., 1996), "embryonic" secondary nucleation, and attrition (Jager et al. 1991). Aggregation models include Brownian motion, laminar shear (Smoluchowski, 1917), turbulent diffusion, and turbulent inertia models (Bramley et al., 1996). While collision frequency is often predicted, the effectiveness of these collisions is not. Another possible reason for the limited predictive capability of these models is that many mechanisms occur simultaneously, leading one researcher to conclude about more successful empirical models that, "Little success has been achieved in relating the variables to specific theoretical mechanisms" (Randolph and Larson, 1988). The poor predictive capability has led to semi-empirical corrections and correlations to bridge the gap between practicality and deep system understanding.

Some techniques for identification of general empirical models have been applied to particulate systems. Specifically, Jager (Jager et al., 1992) has identified linear auto-regressive exogenous (ARX) models for crystallization systems. Rohani (Rohani et al., 1999) added nonlinear neural networks for a crystallization system with size-independent growth, no breakage or aggregation, and purely primary nucleation. By not considering individual particle behavior which depends only on local effects, these models are not portable across experimental systems and provide little extrapolative power.

The most direct method to evaluate particle kinetics is to track individual particles and observe their behavior. Growth of crystals on a window has been studied optically by DeLong (DeLong and Briedis, 1985) and for proteins by Pusey (Pusey and Marshall, 1986). Earlier, Dove studied calcium carbonate *in situ* with scanning force microscopy (Dove and Hochella, 1993). Optical observation of particles *in situ* is being done by Rawlings and Patience (1999). Direct observation has great advantages by providing direct knowledge of the individual particle processes, allowing simultaneous study of all the effects. However, these techniques often require experimental conditions far removed from the conditions of interest, and can require substantial amounts of data to characterize individual particle processes.

First principle models may be abstracted into semi-empirical models by allowing key parameters to vary. Nonlinear optimization can be used to simultaneously determine parameters for growth, nucleation, and aggregation from experimental data. Models capable of capturing the underlying behavior must exist and be chosen for this to succeed, so often the broader class of empirical models is also used. Choices for the models can be found in Jones (Jones et al., 1986) and Eek (Eek et al., 1995). There are many applications to experimental systems (Franck et al., 1988; Jager et al., 1991; Matthews et al., 1996). Often many models are considered, optimized for the data, and compared, with the most successful retained (Bramley et al., 1997; 1996).

Inverse problems arise mathematically when the solution to a differential or integro-differential equation is known, but phenomenological functions in the model are not. While analytic solutions to these problems can be derived in a number of cases, these problems are often ill-conditioned, and noise and discretization of experimental measurements obviates approximate numerical methods. Inverse problem methods are particularly attractive in the absence of *a priori* knowledge of appropriate forms for particle dynamic laws, since the form can be determined directly from the experimental data. Besides, they can also serve to access the veracity of candidate physical models since the result can be compared with the model forms. Inverse problem solution techniques for population dynamics have been long pursued by Ramkrishna and coworkers (Ramkrishna, 2000), including the use of self-similarity to determine aggregation (Wright and Ramkrishna, 1992) and breakage (Sathyagal et al., 1995) laws.

In a steady-state mixed-suspension, mixed product removal reactor (MSMPR), solution of the PBE for the number density $n(l)$ in the absence of aggregation or breakage gives

$$\log n(l) = \log n(0) - \int_0^l \frac{1+\Theta G(l')}{\Theta G(l')} dl' \qquad (1)$$

where Θ is the space-time of the MSMPR, l is a characteristic particle dimension, and $G(l)$ is the growth rate of a particle of size l. This explicit solution allows $G(l)$ to be extracted from $n(l)$ by a transformation given by Sikdar (1997). This gives a size-dependent growth rate directly from the data, free from assumptions about the functional form, though information is gained from only about one set of conditions per experiment.

While this technique is very restrictive, it suggests that a parallel technique for a wider range of experimental systems (batch, semi-batch, or continuous) might be developed, allowing the direct use of experimental data. Before we examine this promise, some preliminaries are in order.

Population Balance

The population balance is the formal relationship between the evolving particle size distribution and the dynamics of individual particles. We consider here a spatially homogeneous (well mixed) particulate system characterized by a single particle dimension, and evolving due to the deterministic processes

$$\frac{\partial n(l,t)}{\partial t} + \frac{\partial [G(l,y)n(l,t)]}{\partial l} = b(l,n,y) \qquad (2)$$

$G(l,y)$ is the growth rate of an individual particle of size l and y is the collection of continuous phase variables that affect particle dynamics. The net rate of the birth of particle size l is given by $b(l,n,y)$. This term includes the effects of aggregation, breakage, and flow across the system boundaries, and may depend on the entire particle-size distribution.

Nucleation defines the boundary condition for the population balance equation

$$n(0,t) = \frac{b_0[t]}{G(0,y)}$$

where $b_0[t] = b_0(n(t),y(t))$ is the nucleation rate. This is a balance between the rate of nucleation, and the particle flux due to growth in phase space.

As this article focuses on particle growth, we have chosen particle diameter as the characteristic dimension. Alternative equivalent formulations may be used that use particle volume or other quantities. Choosing particle volume leads to singularities when evaluating particle growth at near zero sizes, so length is preferred here.

Complete models for these systems require models for the particle processes of growth, nucleation, and aggregation, if present. Additionally, any continuous phase dynamics due to chemical reaction must be known. We will focus here on the determination of the growth rate $G(l,y)$ exclusively.

Inverse Problem Approach

The size- and time-dependence of particle growth are sought directly from experimental data without prior assumption of functional dependence. The inverse problem framework allows this to be done in the context of the entire population, that is, from experiments conducted under the conditions of interest, population dynamics can be reconciled with the laws that dictate individual particle behavior, which may be influenced by the surrounding population. This effective behavior is determined by solving the inverse problem.

As an initial step in the determination, nucleation and growth are considered to vary generally with time rather than with the continuous phase variables $y(t)$. This preserves generality, but requires a second step to determine the exact functional dependence on y. In practice these steps may be combined for the best numerical flexibility, but conceptually it is simpler to view it as a two step process. For each experiment then, the growth rate may be represented as a velocity field $G[l,t] \equiv G(l,y(t))$.

The application of an inverse problem benefits from explicit analytic or approximate solutions. The population balance can be reduced analytically with a method of characteristics. The characteristics of the solution are the trajectories along which the individual particles move, given by $L(t)$ satisfying $dL/dt = G[L,t]$ with initial condition $L(t_0) = l_0$ stemming from either the boundary condition or initial condition for the original PBE. States traceable to the initial condition have $t_0 = 0$ and $l_0 > 0$, those evolving from the boundary condition $l_0 = 0$ and $t_0 > 0$. The separatix is the boundary between these two types of states and is the characteristic corresponding to $t_0 = 0$, $l_0 = 0$. The solution corresponding to a given initial condition will be denoted as $L(t|l_0,t_0)$. Using this transformation, the PDE is reduced to

$$\frac{Dn(l,t)}{Dt} = -n(l,t)\frac{\partial G[l,t]}{\partial l} \tag{3}$$

where D/Dt represents the total derivative along the velocity field $G[l,t]$

$$\frac{Dn(l,t)}{Dt} = \frac{\partial n(l,t)}{\partial t} + G[l,t]\frac{\partial n(l,t)}{\partial l}$$

The solution to Eq. 3 along the characteristics is

$$n(L(t|l_0,t_0),t) = n(l_0,t_0)\exp\left[-\int_{t_0}^{t}\left.\frac{\partial G[l,t']}{\partial l}\right|_{l=L(t'|l_0,t_0)}dt'\right]$$

In using this solution for the forward solution, each (l,t) pair must be traced back to an original (l_0,t_0) corresponding to either the initial $(l_0,0)$ or boundary $(0,t_0)$ condition. This solution shows two effects: a *growth* effect and a *dilation* effect. The growth effect comes from the fact that $n(l,t)$ is directly related to $n(l_0,t_0)$ that the particle experienced at an earlier time, either from the initial or boundary condition. This number density is attenuated by a dilation related to the integrated divergence of the velocity field.

The separation of the two effects is clearer if separable growth is assumed

$$G[l,t] = G_l(l)G_t[t] \tag{4}$$

where $G_t[t]$ contains implicit dependence on $y(t)$. If supersaturation is the only dependence, it may be expressed $G_t[t] = G_\sigma(\sigma)$. The assumption of a separable growth rate is consistent with the literature for a wide range of crystallization and precipitation systems, and will be continued throughout this discussion. The solution under these conditions simplifies considerably and separates the growth and dilation effects. The function $L(t|l_0,t_0)$ is given implicitly by

$$\int_{l_0}^{L(t|l_0,t_0)}\frac{dl}{G_l(l)} = \int_{t_0}^{t}G_t[t]dt \tag{5}$$

and the solution along these characteristics explicitly by

$$n(l,t)G_l(l) = n(l_0,t_0)G_l(l_0) \tag{6}$$

Note that the dilation effect is entirely captured by the size-dependent part of the growth rate $G_l(l)$ and the quantity $G_l(l)n(l,t)$ is conserved along the characteristics. The conservation of this quantity may also be derived directly from the PDE.

These analytic results pertain to the evolution of number density along the characteristics. However, the characteristics themselves depend on the particle growth rate. Fortunately, under many conditions the characteristics can be determined directly from the data. Constant ordering and known particle birth rate are required.

Constant ordering is achieved under conditions of deterministic growth rate (any two particles of the same size exposed to the same conditions grow at the same rate—true for the growth laws discussed here) and well-mixedness (all particles experience the same conditions). Consider two particles, initially $l_2 > l_1$ at $t = 0$. If, at some time later, $l_1 > l_2$ at time t_1, violating constant ordering, continuity requires that at some intermediate time $0 < t < t_1, l_1 = l_2$. However, at this time the particles would have had the same growth rate, a condition that they would keep thereafter, causing contradiction. Therefore, under these conditions, constant ordering is maintained.

If $b(l,n,y)$ is identically zero, a particle initially the N_kth largest in the distribution remains the N_kth largest, corresponding to the kth quantile of the distribution. This can be found each time by integrating the distribution, and the location of this particle identifies a characteristic

$$N_k = \int_{l_k(t)}^{\infty} n(l,t)dl \tag{7}$$

However, if $b(l,n,y)$ is non-zero but known, the number of particles larger than the particle is not constant, but can be determined by a correction

$$N_k(t_2) = N_k(t_1) + \int_{t_1}^{t_2}\int_{l_k(t)}^{\infty} b(l,n,y)dl\,dt \tag{8}$$

$N_k(t)$ is the cumulative over number density corresponding to a particle at $l_k(t)$. Due to the choice of constant cumulative oversize, the birth of particles of zero size does not enter into this correction. Thus, the nucleation rate b_0 does not need to be known, which simplifies the application since newly nucleated particles are difficult to measure.

Equation 8 is generally implicit since $l_k(t_2)$ is not known until $N_k(t_2)$ has been found. These can be found simultaneously. In the case of batch, semi-batch, or continuous systems with well-mixed product removal, there is possible volume change and no aggregation, $b(l,n,y) = -\alpha(t)n(l,t)$ yielding an explicit formula

$$N_k(t_2) = N_k(t_1)\exp\left[-\int_{t_1}^{t_2}\alpha(t)dt\right] \tag{9}$$

Once these corrections have been applied, the remainder of the procedure is identical to the case in which $b = 0$, which will be assumed. Note that this requires the dependence of aggregation and breakage to be known. The curves of $l_k(t)$ corresponding to $N_k(t)$ are *quantiles* of the distribution. Appendix A confirms that the locations of quantiles behave as underlying particles of the same size.

These results suggest a procedure for determining particle growth kinetics. First, experimental data is "counted" to determine the location and number density of quantiles. Second, the number density and particle size along the characteristics are used with analytic solutions from the method of characteristics to find $G[l,t]$.

In the absence of measurement error, this technique can be applied directly to arbitrary precision using a graphical technique, as demonstrated in the next section. However, application to real data is limited by measurement technology which introduces error from sensor noise, sampling variation, and discretization of the particle-size range. With real measurements, graphical techniques can be dominated by error, requiring a more robust numerical technique.

Reducing the infinite dimensionality of the unknown to a finite number of unknowns is accomplished by the expansion of the unknown growth law in a set of basis functions. If appropriate functions are known *a priori*, they may be used, but in this case we will use local Hermite cubic basis functions allowing that different mechanisms may dominate in different size regions. Note that the framework may also be used for parameter estimation in an assumed growth law.

$$G_l(l) = \sum_{i=1}^{p}\alpha_i\phi_i(l) \quad G_t[t] = \sum_{i\text{-}1}^{z} b_i\psi_i(t) \tag{10}$$

The variation of the number density along the characteristics is used with the conserved quantity of Eq. 6 to provide the system of equations

$$n_{1,k}G_l(l_{1,k}) = n_{2,k}G_l(l_{2,k}) = \cdots = n_{m,k}G_l(l_{m,k}) \quad k \in [1,q] \tag{11}$$

where q is the total number of quantiles tracked. This provides a large number of equations which can be used in the determination, although care should be given to maintain independence of the chosen equations. As there is likely little variation in number density between measurements adjacent in time, use of these equations would result in a large relative error in the difference and a high sensitivity to system noise. Instead, a number of intervening time intervals are skipped, based on the amount a characteristic has grown, choosing Δj such that $l_{j+\Delta j,k} - l_{j,k} > \Delta l_{\min}$. Note that Δj varies with j and k in keeping with the local growth rate. This leads to the construction of a number of residuals

$$r_{j,k} = n_{j,k}\sum_{i=1}^{p} a_i\phi_i(l_{j,k}) - n_{j+\Delta j,k}\sum_{i=1}^{p} a_i\phi_i(l_{j+\Delta j,k}) \tag{12}$$

Coefficients of expansion a_i that minimize the residuals are sought. Applying the expansion directly gives

$$r_{j,k} = \sum_{i=1}^{p} a_i\left[n_{j,k}\phi_i(l_{j,k}) - n_{j+\Delta j,k}\phi_i(l_{j+\Delta j,k})\right] \tag{13}$$

These equations are concisely written by letting

$$\phi_{j,k} = \begin{pmatrix} \phi_1(l_{j,k}) \\ \vdots \\ \phi_i(l_{j,k}) \\ \vdots \\ \phi_p(l_{j,k}) \end{pmatrix} \tag{14}$$

then

$$\begin{pmatrix} r_{1,1} \\ \vdots \\ r_{j,k} \\ \vdots \\ r_{m,q} \end{pmatrix} = \begin{pmatrix} n_{1,1}\phi_{1,1}^T - n_{1+\Delta j,1}\phi_{1+\Delta j,1}^T \\ \vdots \\ n_{j,k}\phi_{j,k}^T - n_{j+\Delta j,k}\phi_{j+\Delta j,k}^T \\ \vdots \\ n_{1,1}\phi_{m,q}^T - n_{m+\Delta j,q}\phi_{m+\Delta j,q}^T \end{pmatrix} \cdot a \tag{15}$$

The minimization of residuals occurs at $\boldsymbol{a} = \mathbf{0}$. This is a relic of choosing a degenerate expansion for the growth law. Fixing the product $G_l(l)G_t[t]$ leaves a free multiplicative constant in each factor. To avoid this problem, one entry in $\boldsymbol{a}$ is forced to unity. This is repeated with another choice, and Δl is chosen based on the agreement of the results. A linear least-squares determination is used for the remaining coefficients. Regularization can be applied at this point, but has not been necessary to date.

The determination if a_i has fixed $G_l(l)$, leaving determination of the time dependence ($G_t[t]$). Applying Eq. 6 for the location of each quantile k

$$\int_{l_{j,k}}^{l_{j+1,k}} \frac{dl}{G_l(l)} = \sum_{i=1}^{z} b_i \int_{t_j}^{t_{j+1}} \psi_i(t)dt \qquad (16)$$

These equations form an overdetermined linear system in the coefficients of expansion b_i. Known constraints can be applied to this determination, such as growth and nucleation rates increasing monotonically with supersaturation. There is no free constant since $G_l(l)$ is already determined.

Model validation rests on the agreement of predictions and experimental results. In particulate systems governed by Eq. 2, this prediction requires the initial and boundary conditions. These two steps can be combined into one. As the entire data record from each experiment arises from the initial and boundary conditions according to Eq. 3, each measurement can be traced back to either the initial or boundary condition using the determined growth law. The collapse of these measurements onto the same master curve is equivalent to the prediction of the data, and the dispersion of the collapse is due to experimental or model error. This allows a verification of the model assumptions (deterministic separable growth law, and so on), and also gives the initial and boundary conditions more accurately than using the experimental data nearest to those conditions. These conditions can be used subsequently in the determination of nucleation laws.

The application of this procedure will be shown through the use of two examples. The first is a simple numerical example without measurement discretization or noise and will be approached using a graphical technique. This shows how the evolution of number density along the quantiles can be tied directly to the underlying individual particle growth law. The second example treats a more realistic example where error due to measurement is included. This also shows the subsequent determination of supersaturation dependence.

Numerical Example

The principles behind the theoretical development may be clarified with the use of a numerical example. Figure 1 shows snapshots of a system evolving according to the laws

$$G_l l = 1 + l/6$$

$$G_t[t] = \frac{3}{2}(1 + e^{-t/2})$$

$$n(l,0) = 1 - l$$

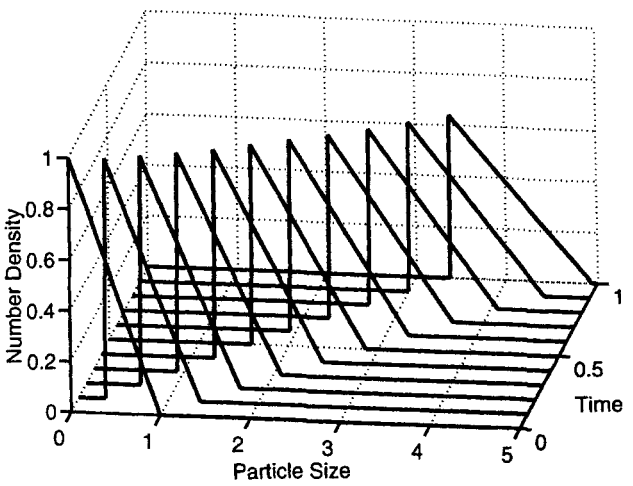

Figure 1. Simulated number density as a function of time for the numerical example.

$$n(0,t) = 0$$

Determining the evolution of the locations of the quantiles of this distribution is straightforward. Figure 2 shows the calculated number oversize, $\int_l^\infty n(l',t)dl'$ along each of the measurements. By taking slices at constant values of the integral, the characteristics are determined. These correspond to the growth trajectories of individual particles, and are plotted in Figure 3.

Once the quantiles are extracted, the number density along each of these characteristics is examined. Since the righthand side of the relationship $n(l,t)/n(l_0,t_0) = G_l(l)/G_l(l_0)$ is the same for all particle trajectories, plots of $n(L,t)$ vs. l should differ by only a multiplicative constant, and be proportional to $1/G_l(l)$. This is borne out in Figure 4. This suggests the construction of G_l from the reciprocal of these graphs.

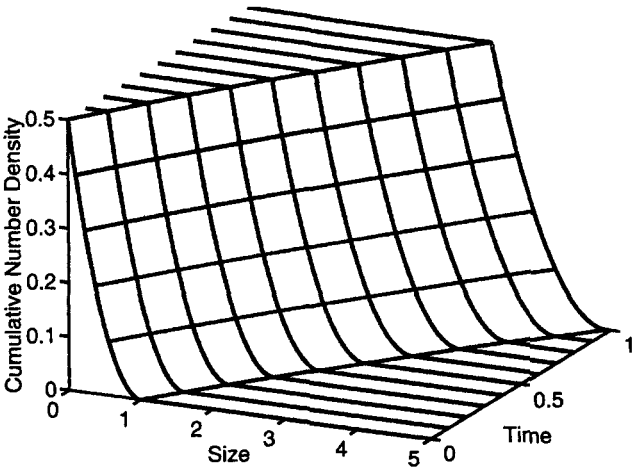

Figure 2. Integrated number density with lines of constant number oversize for numerical example.

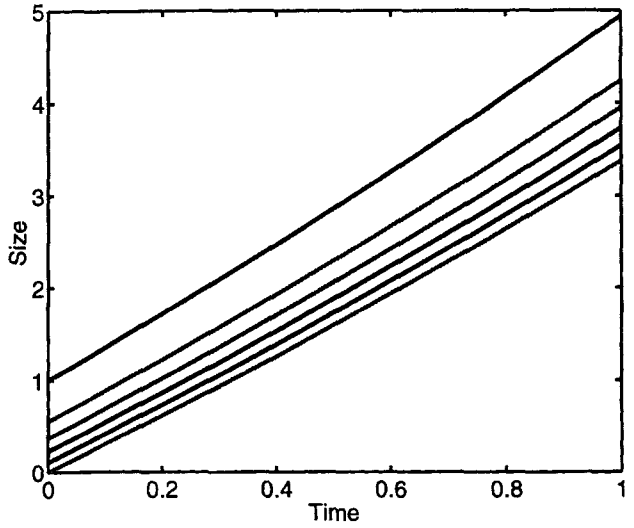

Figure 3. Location of characteristics obtained by projecting lines of constant number oversize onto the t-l plane from numerical example.

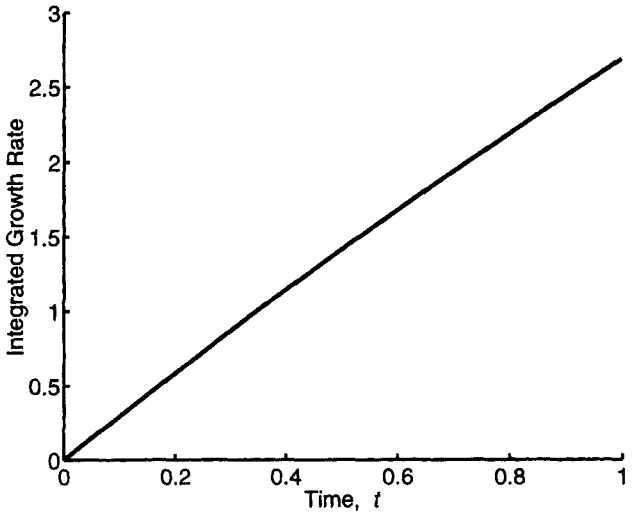

Figure 5. Collapsed curves obtained from $\int^{l_t} dl/G_l(l(t))$ with $l(t)$ along the extracted characteristics.

This is equal to $\int_0^t G_t[t']dt'$.

Once G_l is determined, the amount of particle growth can be used to determine G_t. In Figure 5, the quantity

$$\int_{l_0}^{l(t)} \frac{dl}{G_l(l)} = \int_0^t G_t[t]dt$$

is plotted as a function of time by computing the first integral of the now known size dependence. Notice that all of the curves collapse onto a single curve, the derivative of which gives precisely the time dependence of growth.

While illustrating the underlying principles and producing effectively infinite dimensional results, this graphical technique is impractical in practice due to measurement and process noise. The operations of collapsing curves along characteristics and differentiating the time curve become ill-conditioned. For a practical application, the numerical approach described above may be required.

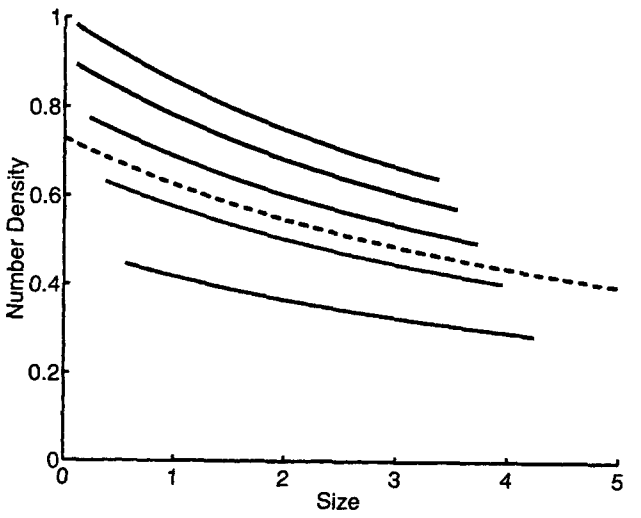

Figure 4. Number density along characteristics, plotted along with the reciprocal of the growth rate law (dashed) = $1/G_l(l)$.

Application to Precipitation System

This example follows the application of the technique to a simulated precipitation system. The "raw" data shown in Figure 6 were generated using Galerkin's method on finite elements with the growth law given by

$$G(l,\sigma) = \sigma^2\left[1-\frac{1}{2}\exp\left(-\frac{l}{2}\right)\right]\left[\frac{1}{2}-\frac{1}{2\pi}\arctan\left(\frac{l-16}{2}\right)\right] \tag{17}$$

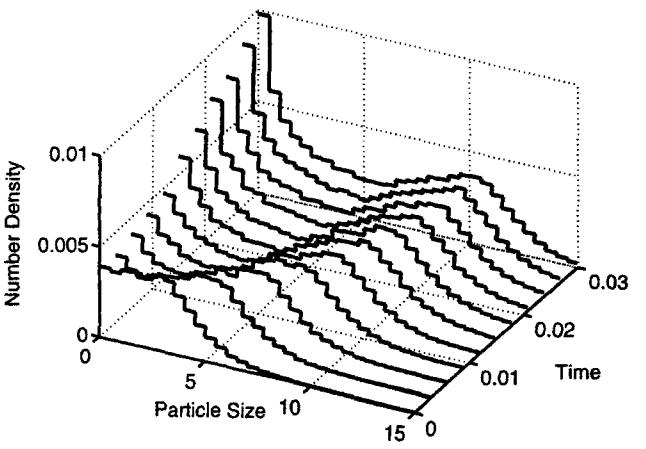

Figure 6. Discretized simulation data for precipitation.

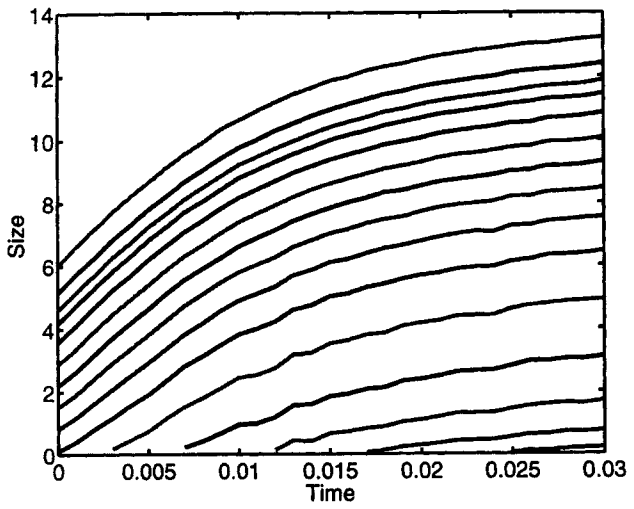

Figure 7. Quantiles (characteristics) obtained from constant over cumulative numbers from Example 2.

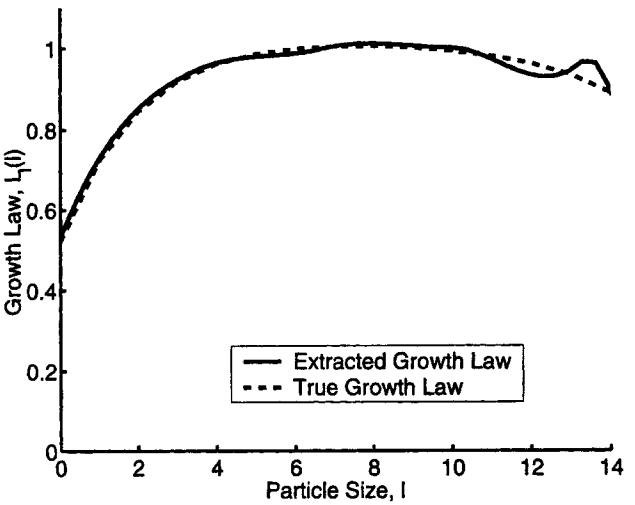

Figure 8. Determined and true size-dependent growth law from Example 2.

The growth law displays deviations from constant size dependence both at small and large sizes. The deviation at small sizes mimics the behavior postulated by Abegg et al. (1968) in explaining observed growth rate deviations at low sizes. Another deviation applies to large particle sizes based on a model for particle attrition by Jager et al. (1991).

To simulate more realistic measurement data, the solution was distcretized in size and time and each data point was corrupted with normally distributed noise with a standard deviation of 3% of the mean.

The number of quantiles tracked ranged from 28 at the beginning of the simulation to 43 at the end. The number was chosen as approximately half the number of measurement points covered by the distribution. Quantiles closer in size than the discretization width will provide no additional data, and since two quantities are computed from each quantile (the size and number density), additional quantiles are unnecessary. Figure 7 shows the location of these quantiles. With nucleation, it is clear that only by counting down from large particle sizes will the same particles be found. Note also that characteristics corresponding to over 100% of the original population are included which trace back to the boundary condition of newly nucleated particles.

For expansion of $G_l(l)$, the size-dependent portion of the growth law, Hermite cubic basis function with node points at $l = (0,3.33,6.67,\ldots,16.67)$ were chosen for ten unknown coefficients of expansion. The minimum limit of separation, $\Delta l_{\min} = 2$ was chosen using two criteria. First, it is over half the size discretization of the trial functions so that the residual equations relate different unknown coefficients of expansion. Second, this value gives the best agreement between solutions computed selecting different coefficients to be unity. These choices result in an overdetermined system of 422 equations, the residuals of which are minimized with no further weighting. The resulting growth law is shown in Figure 8. When compared with the simulated growth law, error is evident with increasing particle size due to the few particles that attained this size in the data record.

Hermite cubics were again chosen for the time-dependent growth law, with nodes placed at $t = 0,.015,.03$, for six unknown coefficients. Integration of the reciprocal of the determined size dependence and the trial functions are used to compute the residual equations. A total of 1,126 equations are generated, and optimized giving the results in Figure 9.

From this determination of the growth rate as a function of time to dependence on other quantities is a straightforward step. Figure 10 shows the growth rate plotted against an independently measured supersaturation. While this two-step procedure is the most general, data from multiple experiments are more easily reconciled if estimates of the variables affecting the driving force are available, replacing $\psi_i(t)$ in Eq. 16 with $\psi_i[y]$ ($\psi_i[\sigma]$) and interpolating $y(\sigma)$ between measurements. For a multidimensional system where the key variables are unknown, direct knowledge of $G_t[t]$ may be more useful.

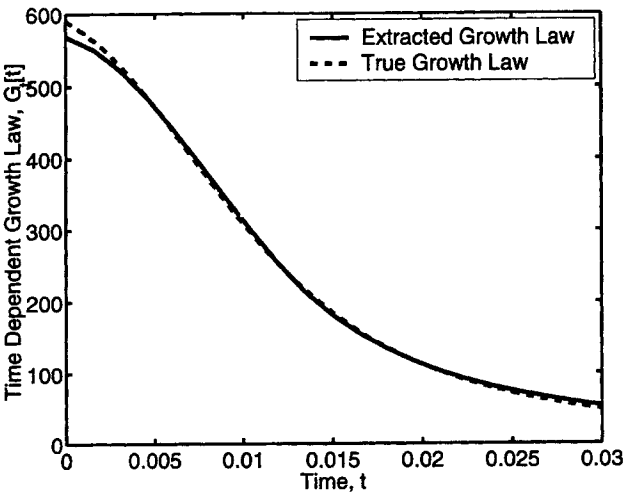

Figure 9. Determined and actual time-dependent growth law for Example 2.

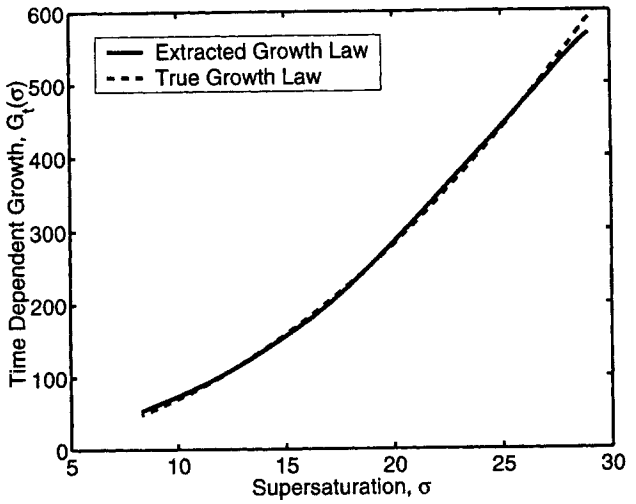

Figure 10. Time-dependent growth law plotted against measured supersaturation (3% noise added) for Example 2.

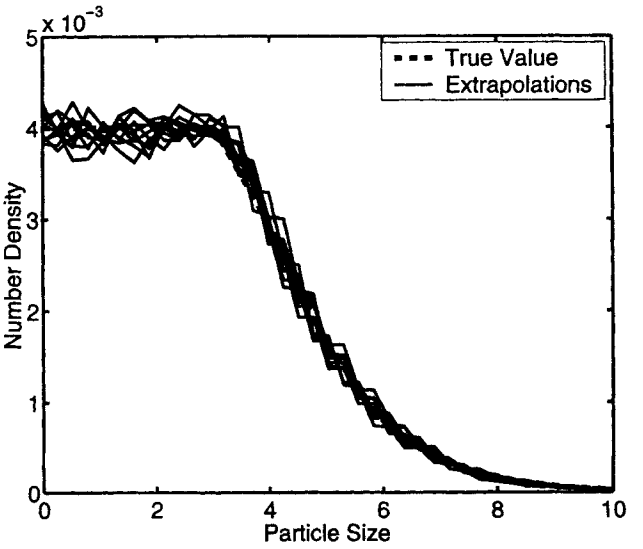

Figure 12. Simulated measurements extrapolated to time zero to obtain initial size distribution, plotted with true initial condition for Example 2.

In practice, the true growth laws will be unknown so the determined growth laws are verified by prediction of the measured data based on solution of the population balance equation. Before this can be done either analytically or numerically, both the boundary and initial conditions are required. These could be fitted with basis function expansions in a similar manner to the growth law, but a combined approach allows simultaneous verification and construction of the initial and boundary conditions. The analytic solution of the method of characteristics is used, but beginning with each measured distribution and solving for the solutions at size zero and time zero. These are plotted individually in Figures 11 and 12. The collapse agrees with the initial and boundary conditions used for simulation, but the evaluation of the growth law comes from the collapse onto single curves. This collapse gives both the values of the initial distribution and nucleation rate, and the scatter corresponds to the ability to predict the measured data. The measurements have been effectively projected onto common axes.

The determined boundary condition gives the nucleation rate directly, and can be used in further modeling to determine primary or secondary nucleation laws.

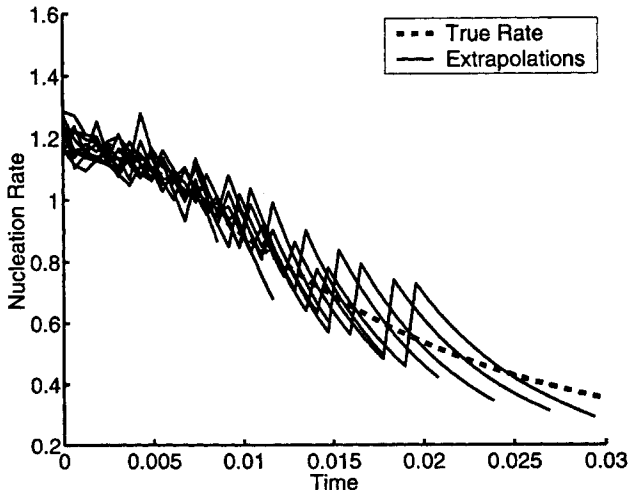

Figure 11. Simulated measurements extrapolated to size zero to obtain nucleation rate plotted with true nucleation rate for Example 2.

Conclusions

We have presented a technique for the determination of deterministic growth laws directly from experimental data. This technique uses experimental data to determine the underlying growth laws, both qualitatively and quantitatively, which was information previously unavailable from general experiments.

This determination of general dependency can be used for a number of purposes. The most obvious is a direct empirical model, but independent choice and verification of candidate models is powerful, being able to define the range over which models hold. This can also give insight into the underlying physical behavior, as a direct model makes it more likely that dependences relating to complementary mechanisms will be identified.

While a direct empirical model with local basis functions does not suggest extrapolation to unmeasured particle sizes, the subsequent identification of the law with basic mechanisms does allow extrapolation. Comparison with the underlying law also suggests the quality that may be obtained from extrapolation.

Finally, general models allow a better understanding of the underlying physics. Having available the form of a size-dependent growth law may suggest and motivate the development of laws for new mechanisms and improve the understanding of particulate systems.

Acknowledgments

The authors wish to thank the Computer Integrated Process Operations Consortium (CIPAC) at Purdue University for financial support. Alan Mahoney gratefully acknowledges support from the McAllister and Andrews Fellowships.

Notation

a_i = coefficients of basis function expansion for $G_l(l)$
$b(l,n,y)$ = net production rate of size l particles, particles/m/m^3/s
$b_0[t]$ = nucleation rate, particles/m^3/s
$G(l,y)$ = individual particle growth rate, m/s
$G[l,t]$ = individual particle growth rate, as an apparent function of time, m/s
$G_l(l)$ = size-dependence of degenerate growth rate
$G_t[t]$ = time-dependence of degenerate growth rate
l = characteristic particle length, m
$l_k(t)$ = size of particle corresponding to quantile k at time t, m
$l_{j,k}$ = extracted location of quantile k at jth measurement, m
$L(t|l_0,t_0)$ = particle size along the characteristic defined by t_0 and l_0, m
n = length based number density, particles/m/m^3
$n_{j,k}$ = number density at $l_{j,k}$ and t_j, particles/m/m^3
$N_k(t)$ = cumulative over number density corresponding to quantile k, particles/m^3
p = total number of basis functions, ϕ_i, chosen for size expansion
q = number of chosen quantiles
$r_{j,k}$ = residual from dilation effect corresponding to quantile j at measurement k
t = time, s
t_j = time of jth experimental measurement, s
$[t]$ = denotes an apparent general time dependence
y = vector containing continuous phase variables, such as supersaturation, σ
z = total number of basis functions, ψ_i, chosen for time expansion
$\alpha(t)$ = reciprocal of the space time in a continuous system (not necessarily at steady state), s^{-1}
Δj = difference in time measurements used for computing an individual residual $r_{j,k}$
Δl = difference in length measurements used for computing residuals $r_{j,k}$
Θ = space-time of a continuous system, s
σ = supersaturation, dimensionless
$\phi_i(l)$ = basis functions for expansion of $G_l(l)$
$\phi_{j,k}$ = vector if ϕ_i evaluated at $l_{j,k}$
$\psi_i(t)$ = basis functions for expansion of $G_t[t]$
i = index for basis functions
j = index for measurement times
k = index for chosen quantiles

Literature Cited

Abegg, C. F., J. D. Stevens, and M. A. Larson, "Crystal Size Distributions in Continuous Crystallizers when Growth Rate is Size Dependent," *AIChE J.*, **14**, 118 (1968).

Bramley, A. S., M. J. Hounslow, and R. L. Ryall, "Aggregation during Precipitation from Solution. Kinetics for Calcium Oxalate Monohydrate," *Chem. Eng. Sci.*, **52**, 747 (1997).

Bramley, A. S., M. J. Hounslow, and R. L. Ryall, "Aggregation during Precipitation from Solution: A Method for Extracting Rates from Experimental Data," *J. Colloid Interf. Sci.*, **183**, 155 (1996).

DeLong, J. D., and D. Briedis, "A Technique for the Study of Growth Rates of Single Crystals of Sparingly Soluble Salts," *J. Cryst. Growth*, **71** 689 (1985).

Dove, P. M., and M. F. Hochella, "Determination of Calcite Surface-Reaction Processes-in situ Observations by Scanning Force Microscopy," *Abstr. Pap. Am. Chem. S.*, **205**, 135 GEOC (Mar. 1993).

Eek, R. A., S. Dijkstra, and G. M. van Rosmalen, "Dynamic Modeling of Suspension Crystallizers, Using Experimental Data," *AIChE J.*, **41**, 571 (Mar. 1995).

Franck, R., R. David, J. Villermaux, and J. P. Klien, "Crystallization and Precipitation Engineering: II. A Chemical Reaction Engineering Approach to Salicylic Acid Precipitation Modelling of Batch Kinetics and Application to Continuous Operation," *Chem. Eng. Sci.*, **43**, 69 (1988).

Gómez-Morales, J., J. Torrent-Burgués, and R. Rodríquez-Clemente, "Nucleation of Calcium Carbonate at Different Initial pH Conditions," *J. Cryst. Growth*, **169**, 331 (Nov. 1996).

House, W. A., "Kinetics of Crystallization of Calcite from Calcium Bicarbonate Solutions," *J. Chem. Soc., Faraday Trans. 1*, **77**, 341 (1981).

Jager, J., S. de Wolf, H. J. M. Kramer, and E. J. de Jong, "Estimation of Nucleation and Attrition Kinetics from CSD-Transients in a Continuous Crystallizer," *Trans. Inst. Chem. Eng.*, **69** 53 (Jan. 1991).

Jager, J., H. J. M. Kramer, E. J. deJong, S. de Wolf, O. H. Bosgra, A. Boxman, H. G. Merkus, and B. Scarlett, "Control of Industrial Crystallizers," *Powder Technol.*, **69** 11 (1992).

Jones, A. G., J. Budz, and J. W. Mullin, "Crystallization Kinetics of Potassium Sulfate in an MSMPR Agitated Vessel," *AIChE J.*, **32**, 2002 (Dec. 1986).

Matthews, H. B., S. M. Miller, and J. B. Rawlings, "Model Identification for Crystallization: Theory and Experimental Verification," *Powder Technol.*, **88**, 227 (Sept. 1996).

Nielsen, A. E., "Electrolyte Crystal Growth Mechanisms," *J. Cryst. Growth*, **67** 289 (1984).

Pusey, M. L., and G. C. Marshall, "An Apparatus for Protein Crystal-Growth Studies," *Anal. Biochem.*, **158**, 50 (Oct. 1986).

Ramkrishna, D., *Population Balances: Theory and Applications to Particulate Systems in Engineering*, Academic Press, San Diego (2000).

Randolph, A. D., and M. A. Larson, *Theory of Particulate Processes*, second ed., Academic Press, San Diego, CA (1988).

Rawlings, J. B., and D. B. Patience, "On-line Monitoring and Control of Crystal Size and Shape," *Ann. Meeting of Int. Fine Particle Research Institute*, Somerset, NJ (Jun. 1999).

Rohani, S., M. Haeri, and H. C. Wood, "Modeling and Control of a Continuous Crystallization Process: 1. Linear and Non-linear Modeling," *Comp. Chem. Eng.*, **23**, 263 (1999).

Sathyagal, A. N., D. Ramkrishna, and G. Narsimhan, "Solution of Inverse Problems in Population Balances: II. Particle Break-up," *Comp. Chem. Eng.*, **19**, 437 (1995).

Sikdar, S. K., "Size-Dependent Growth Rate from Curved Log $n(L)$ vs. L Steady State Data," *Ind. Eng. Chem. Fundam.*, **16**, 390 (1977).

Smoluchowski, M. V., "Mathematical Theory of the Kinetics of the Coagulation of Colloidal Solutions," *Z. Phys. Chem.*, **92**, 129 (1917).

Tai, C. Y., C.-S. Cheng, and Y.-C. Huang, "Interpretation of Crystal Growth Rate Data Using a Modified Two-Step Model," *J. Cryst. Growth*, **123**, 236 (1992).

Wright, H., and D. Ramkrishna, "Solutions of Inverse Problems in Population Balances: I. Aggregation Kinetics," *Comp. Chem. Eng.*, **16**, 1019 (1992).

Equivalence of Quantiles and Characteristics

The location of the kth quantile $l_k(t)$ is such that for constant N_k

$$N_k = \int_{l_k(t)}^{\infty} n(l,t)\,dl \tag{18}$$

Taking the time derivative of both sides gives

$$0 = \frac{dN_k}{dt} = -\int_{l_k(t)}^{\infty} \frac{\partial n(l,t)}{\partial t}\,dl - i_k(t)n(l,t) \tag{19}$$

Where $i_k(t) = dl_k/dt$. Substituting the population balance $\partial n/\partial t = -\partial/\partial l[G[l,t]n(l,t)]$ from the population balance and simplifying

$$i_k(t) = G(l_k(t),t) \tag{20}$$

Since the rate of change for the location of the quantile is identical to that of a particle of the same size, and this rate does not vanish, the quantile moves exactly as a particle of the same size.

Manuscript received Oct. 31, 2000, and revision received Aug. 20, 2001.